A numerical study of non-Newtonian transient elastohydrodynamic lubrication of metal-on-metal hip prostheses

L Gao[a)], D Dowson[b)], RW Hewson[a)]

a) Department of Aeronautics, Imperial College London, London, UK, SW7 2AZ
b) School of Mechanical Engineering, University of Leeds, Leeds, UK, LS2 9JT
Leiming.gao@gmail.com

Keywords:
Non-Newtonian, shear-thinning, transient, EHL, metal-on-metal hip prosthesis

Abstract

This paper presents a comprehensive numerical study of transient non-Newtonian elastohydrodynamic lubrication of metal-on-metal hip prosthesis subjected to two different gait cycles. The shear-thinning property of the synovial fluid was found to have a significant effect on the lubricating film, in terms of both the magnitude and location of the minimum film thickness, and more generally the film thickness distribution. A range of clearances between the acetabular cup and femoral head were investigated and the shear-thinning effect was more pronounced in the hip replacements with smaller clearances.

1 INTRODUCTION

1.1 Historical background

Total joint replacement (THR) has been hailed as the major development in orthopaedic surgery in the past century. In the 1950's two material pairs were investigated; metal-on-metal (MoM) [1] and metal-on-polymer [2]. In the latter case the polymeric acetabular cup was initially made from polytetrafluoroethylene (ptfe/teflon), a bearing material with the lowest known coefficient of friction, but it

soon emerged that its wear resistance was inadequate and so an alternative polymer, ultra high molecular weight polyethylene (UHMWPE) was adopted. The Charnley total hip replacement dominated the next half century or so and is still the first choice for many surgeons. In due course interest arose in alternative material combinations including;

- Ceramic heads in UHMWPE cups
- Ceramic heads in ceramic cups
- Metal heads in metal cups

It has been recognized that severe wear and aseptic loosening caused by polyethylene wear particles were the main reasons for the failure of metal-on-UHMWPE implants [3]. To avoid polyethylene wear particles MoM material combinations have attracted more attention in the mid 1980's due to its high wear resistance. The long-term survival in some patients encouraged its usage particularly in younger and more active patients. However in recent years, concerns have arisen regarding high wear of some implant designs [4, 5], and, in general toxicities of metal wear particles and metal ions that may transport outside the joint capsule and cause adverse tissue reactions both locally and remotely [6]. Despite the potential biocompatibility issues associated with metal debris, some MoM hip implants have exhibited encouraging tribological and clinical performance.

It is interesting to note that there has been a move away from hard-on-soft material pairs to hard-on-hard combinations, even though nature did not promote the latter solution. The use of soft-on-soft material pairs, reflecting the cartilage-on-cartilage situation in natural joints is also attracting interest, while at the other end of the scale hard, wear resisting coatings are being developed [7].

If hard-on-hard material pairs are used it is essential to minimize asperity interactions and wear. The components are manufactured with high accuracy and the smallest realistic roughness. For metal-on-metal combinations, the femoral head diameters

range from about (28-62) mm, the composite surface roughness (R_a) values for both heads and cups are often in the range (5-20) nm, while diametrical clearances range from about (50-300) μm. When implanted, surface scratches may result in local higher roughness compared with the starting values. There are conflicting reports on the influence of, "running-in" upon the surface roughness in MoM hip joints.

The transmission of load during the varied activities of daily life needs to be achieved with minimum aggressive interaction between femoral heads and acetabular cups. Such interactions can influence both traditional and well recognized wear mechanisms (abrasion; adhesion and fatigue) and it is now recognized that tribo-corrosion can contribute significantly to material loss [8]. In order to minimize wear and tribo-corrosion it is necessary to support as much load as possible by fluid-film (elastohydrodynamic) lubrication and to minimize boundary or mixed lubrication action.

The aim of the current study is to provide a more accurate lubrication model, by addressing the shear-thinning properties of the synovial fluid.

The variation of loads and entraining velocities within one cycle; the developing profiles of the bearing surfaces; the environmental operating conditions and the rheological characteristics of the lubricant (synovial fluid) all need to be modelled and it is the role of the latter which is a major feature of the present paper.

1.2 Background to elastohydrodynamic lubrication analysis of hip replacements

Analytical and numerical solutions to the elastohydrodynamic lubrication problem for engineering components emerged in the second half of the 20th Century. The principal findings were that, for engineering lubricants and steady state conditions, the minimum film thickness was very little affected by load, and that the magnitude of the separation between smooth solids was largely determined by the lubricant

viscosity and entraining velocity. Simple expressions for minimum film thickness were developed for both line and point contacts and these have been widely used by designers of highly stressed machine components such as gears, rolling element bearings. The magnitudes of the calculated minimum film thicknesses were significantly greater than those derived from Reynolds equation for rigid solids, often by one or two orders of magnitude.

Elastohydrodynamic action plays a major role in the fluid-film lubrication of natural synovial joints and their man-made replacements. The importance of squeeze film action in damping out the otherwise rapid cyclic changes in film pressures and film thickness was demonstrated by Jin and Dowson [9] and Dowson et al. [10] from both theoretical simulations and experimental measurements. It has long been recognized that synovial fluid is a highly non-Newtonian fluid, but successful incorporation of the spectacular effect of shear rate upon viscosity in numerical solutions to the hip joint replacement problem has been delayed while viscometers have been developed to measure lubricant viscosity for shear rates over six or seven orders of magnitude. The possible role of other constituents of synovial fluid, such as proteins [10, 11] is not considered in the present paper. However, the effect of shear upon lubricant viscosity over the full range of shear rates encountered in total replacement hip joints has been assessed for the first time.

1.3 Literature review of numerical non-Newtonian EHL study of hip joints

In many numerical simulations of artificial hip replacement lubrication, the shear-thinning effect of the joint's synovial fluid has been neglected [12-20], i.e., the fluid was assumed to be Newtonian, with a viscosity similar to water. The primary reason given for this assumption is that the shear-thinning effect was assumed to be negligible when the shear rate was in a high range of between 10^5 and 10^7 s^{-1}, governed by the range hip joints typically experience during walking cycles [21]. There are limited numerical studies that investigate the rheology of joint synovial

fluid. The most significant of these are described below. Wang et al. [22] developed a shear thinning EHL model of metal-on-metal hip implants under steady state conditions, with the rheological parameters obtained from experimental data presented by Yao et al. [21], and little difference in pressure and film thickness was found between the solutions of Newtonian and non-Newtonian models. In their study [22] only a relatively small range of shear rates were investigated. Tichy and Bou-Said [23] studied the non-Newtonian viscoelastic properties of the synovial fluid in pure-squeezing of hip joint replacements in gait cycles. Their rheological model was developed based on the Phan-Thien and Tanner (PTT) model which is often used to describe polymer solutions [24]. Meziane et al. [25] further developed the PTT viscoelastic model to simulate a complete hydrodynamic lubrication of hip implants subject to a walking cycle. Both of the studies [23, 25] have found that the non-Newtonian property of the joint synovial fluid has significant effect on the lubrication, particularly when the squeeze film effect is present, as it is in the transient walking cycle.

This paper addresses the above differences in the non-Newtonian effects, by presenting a comprehensive numerical analysis of the transient EHL of metal-on-metal hip implants subject to different walking cycles. These are described by a simplified walking pattern and a more complex physiological walking pattern, with the shear-thinning properties of the synovial fluid addressed. In the results, the elastohydrodynamic pressure and film thickness are predicted, with particular attention paid to the magnitude and location of the minimum film thickness in a walking cycle. These results are compared with the corresponding Newtonian results to investigate the shear thinning effect, for a range of the design clearances between the femoral head and the acetabula cup.

2 Materials and Numerical Method

A total hip replacement made from cobalt chromium alloy with a femoral head diameter of 36 mm and, diametrical clearances of (50 -150) μm between the head and the cup, was investigated in the analysis. The cup was assumed to be firmly fixed to the pelvic bone through an equivalent layer representing bone and/or fixation cement. The material and geometrical parameters are presented in Table 1. An illustration of the hip implant and associated three-dimensional loading and motions is shown in Fig. 1. Two loading and motion patterns of walking cycles were considered in this study, a Leeds ProSim hip simulator [26] and 3 dimensional physiological walking pattern described by Bergmann et al. [27], as shown in Fig. 2. Cup inclination angles of both 0 and 45 degrees were considered in the analysis for the hip simulator walking cycles, and the inclination angle of 45 degrees was considered in the physiological walking cycle.

2.1 Viscosity Model of Synovial Fluid

Numerous measurements have revealed high values of synovial fluid viscosity, typically ranging from about (10^4-10^5) mPas, at very low shear rates. Furthermore, Cooke et al [28] drew attention to the considerable variation from one subject to another, and even within one subject, depending upon the severity of arthritic disease. Joint disease reduced the effect of shear rate upon viscosity, with normal joint fluid exhibiting the greatest non-Newtonian effects, followed by fluid from osteo- and rheumatoid arthritic joints. This has prompted some investigators to suggest that determination of the magnitude of non-Newtonian characteristics of synovial fluid may be used as an indication of the severity of joint disease.

In hip joint replacements mean shear rates (≈u/h) are typically in the range (10^6-10^7) 1/s and under these circumstances the viscosity attains a near constant value which differs little from that of water. The values adopted for this very high shear rate viscosity generally range from about (1-5) times that of water (0.692 mPas at 37°C).

In this study the viscosity of synovial fluid at any point in the elastohydrodynamic

lubricating film was based upon a relationship of the form proposed by Cross [29].

$$\eta = \eta_\infty + \frac{\eta_0 - \eta_\infty}{1+\alpha(\dot{\gamma})^\beta} \quad (1)$$

Cross proposed a value of (2/3) for *(β)* and with values of viscosity being measured at very low and very high shear rates, the value of *($\propto$)* could be calculated at intermediate shear rates. In the present exercise the limiting shear rate values of viscosity adopted were (η_0=40,000 mPas) and (η_∞=0.9 mPas). Recorded values of viscosity for synovial fluid from eight different sources suggested that a fair representation of viscosity over the very large range of shear rates encountered in joint replacements was given with $\propto$ = 9.54 and β = 0.73. The latter value is similar to, but slightly higher than the value 0.67 adopted by Cross.

The pressure variation across the lubricating film thickness was neglected due to the very thin films considered. An average shear rate $(\dot{\gamma})$ was adopted and calculated as the ratio of relative surface velocity to film thickness. Although the shear rate varies across the film, the main purpose of this initial paper was to explore the influence of viscosity variation throughout a complete loading cycle. The variation of shear rate across the film in Poiseuille flow modified the Couette shear rate in positive and negative directions but it is the absolute value of the shear rate that affects the viscosity. The resulting non-linear effect did not, however, appear to play a significant role when applied over the complete domain, as demonstrated by Wang et al. [22].

$$\dot{\gamma} = \frac{v}{h} \quad (2)$$

with the velocity (*v*) given by:

$$v = \sqrt{v_\theta^2 + v_\varphi^2} \quad (3)$$

$$\begin{cases} v_\theta = -R_c\omega_x \sin\varphi + R_c\omega_y \cos\varphi \\ v_\varphi = -R_c\omega_x \cos\varphi\cos\theta - R_c\omega_y \sin\varphi\cos\theta + R_c\omega_z \sin\theta \end{cases} \quad (4)$$

In the current study, the viscosity at the infinite shear rate of 0.9 mPas was used to obtain the corresponding Newtonian results for comparison.

2.2 Elastohydrodynamic Lubrication Formulation

The Reynolds equation was used to describe the lubricated flow formulated in spherical coordinates [13]:

$$\begin{aligned}&\frac{\partial}{\partial\varphi}\left(\frac{h^3}{\eta}\frac{\partial p}{\partial\varphi}\right)+\sin\theta\frac{\partial}{\partial\theta}\left(\frac{h^3}{\eta}\sin\theta\frac{\partial p}{\partial\theta}\right)\\&=6R_C^2\sin\theta\left[\begin{array}{l}-\omega_x\left(\sin\varphi\sin\theta\dfrac{\partial h}{\partial\theta}+\cos\varphi\cos\theta\dfrac{\partial h}{\partial\varphi}\right)\\+\omega_y\left(\cos\varphi\sin\theta\dfrac{\partial h}{\partial\theta}-\sin\varphi\cos\theta\dfrac{\partial h}{\partial\varphi}\right)\\+\omega_z\sin\theta\dfrac{\partial h}{\partial\varphi}\end{array}\right]\\&+12R_C^2\sin^2\theta\frac{\partial h}{\partial t}\end{aligned} \tag{5}$$

where, φ and θ are spherical coordinates as shown in Fig. 3; $\omega_{x,\,y,\,z}$ represent the angular velocities of FE, IER and AA motions respectively, as defined in Fig. 1. Considering the angle of cup inclination (β_0), the inlet and outlet boundaries of the lubrication domain were defined as:

$$\begin{cases}\theta_{in}=0,\theta_{out}=\pi\\\varphi_{in}=\beta_0,\varphi_{out}=\beta_0+\pi\end{cases} \tag{6}$$

The hydrodynamic pressure (p) was assumed to be zero at both the inlet and the outlet boundaries. The cavitation boundary condition was achieved by setting the obtained negative pressure to zero during the relaxation process in the entire calculation domain.

The film thickness (h) including both rigid and elastic deformation (δ) between the

two bearing surfaces, was calculated as:

$$h(\varphi,\theta) = c/2 - e_x \sin\theta\cos\varphi - e_y \sin\theta\sin\varphi - e_z \cos\theta + \delta(\varphi,\theta) \tag{7}$$

$$\delta(\varphi,\theta) = \int_{\varphi}\int_{\theta} K(\varphi-\varphi',\theta-\theta',\theta_m)\, p(\varphi',\theta')\, d\theta\, d\varphi \tag{8}$$

An equivalent spherical discrete convolution (ESDC) technique [30] and the multi-level multi-integration (MLMI) were adopted to obtain the surface elastic deformation. *K* denotes the displacement influence coefficient of the elastic surfaces and θ_m denotes a fixed mean latitude [30]. The external 3D loading components $w_{x,y,z}$ were balanced by the hydrodynamic pressure integrated with respect to the corresponding axes:

$$w_{x,y,z} = R_C^2 \int_{\varphi}\int_{\theta} p_{x,y,z}\, d\theta\, d\varphi \tag{9}$$

where the pressure components in three Cartesian coordinate directions are expressed as:

$$\begin{cases} p_x = p\sin^2\theta\cos\varphi \\ p_y = p\sin^2\theta\sin\varphi \\ p_z = p\sin\theta\cos\theta \end{cases} \tag{10}$$

The governing equations were made dimensionless in order to improve numerical stability and facilitate convergence. The equations were subsequently transformed into discrete forms using the finite difference schemes. Gauss-Seidel relaxation was employed for pressure iteration in the Reynolds equation, and the multi-grid techniques were employed. The details of these numerical procedures to solve the equations can be found in [13].

3 Results

The numerical simulation started from an initial steady-state solution as at the first time step in the walking cycle, after three walking cycles the EHL solutions converged to a periodic solution. All the results presented in this paper were obtained for periodic walking cycles. The magnitude of the minimum film thickness and its

location in the walking cycle were compared between the Newtonian and non-Newtonian fluids, for a range of diametrical clearances between 50 μm and 150 μm. Results for the two loading patterns considered, i.e., hip simulator and physiological conditions respectively, are shown in Fig. 4 (a) and (b).

For the case of a diametrical clearance of 100 μm, more results are shown in Figs. 5-8. The variations of the minimum and central film thickness in a walking cycle are presented in Fig. 5. Fig. 5 a) and b) shows the results for the hip simulator with the cup inclination angle of 45 degrees and zero respectively; Fig. 5 c) shows the results for the physiological load pattern. It is found that the cup inclination angle does not affect much the predicted film thickness as long as the main loading area is far away from the rim of the acetabular cup. For example, for the diametrical clearance of 100 μm the minimum and maximum values of the minimum film thicknesses in the hip simulator cycle for the two solutions vary by only 3.7% and 1.6% for the Newtonian solutions, 4.5% and 0.8% for the non-Newtonian solutions. The film thickness contours at two time steps (0.2 s and 0.64 s) occurring during the stance phase and swing phase respectively for the hip simulator pattern are plotted in Fig. 6 (At 0.64 s the reversal rotation resulted in zero velocity). The film thickness contours at 0.55 s and 1.1 s, occurring during the loading and swing phases respectively in the physiological walking pattern are plotted in Fig. 7. The Newtonian and non-Newtonian film thickness profiles on a cross-section at two different time steps (same as Fig. 6) in a walking cycle are compared in Fig. 8. The non-Newtonian viscosity contours at specific time steps are shown in Fig. 9, along with the minimum viscosity through the two different gait cycles in Fig. 10.

4 Discussion

The effect of shear thinning on the overall performance of an artificial hip joint is illustrated in Fig. 4. Figs. (4a) and (4b) show how the minimum film thickness varies with the diametrical clearance of the joint. It can be seen from these results that the

minimum film thickness predicted for the shear thinning fluid properties is greater than that of the constant viscosity fluid in all cases. This is not wholly unexpected as the Newtonian fluid case has the same viscosity as the high shear rate limit of the non-Newtonian case, resulting in the fluid viscosity always being greater or equal to the viscosity of the Newtonian case. What is perhaps of greater interest is the transient location of the minimum film thickness in the gait cycle. Indeed, as will be seen later (Fig. 5), the minimum film thickness variation in the gait cycle is significantly different for the two rheological cases examined. Unlike the actual value of the minimum film thickness which has a near constant difference between the two rheologies (Figs. (4a) and (4b)), the location of the minimum film thickness throughout the entire gait cycle does not show such a consistent trend with the minimum film thickness occurring at different times during the gait cycle.

For the case when a more realistic gait cycle is examined, i.e. one where the motion is not constrained in a single plane, the location in the gait cycle of the minimum film thickness calculated for both the rheological models are reasonably similar to each other (note the difference in ordinate axis scaling between Figs. 4(a) and 4(b). The smaller difference between the locations of this minimum film thickness can be attributed to a more rapidly changing minimum film thickness variation with time for the simulator than for the more realistic physiological gait cycle. This can be seen in Fig. 5, where the variation in film thickness for the two cycles is shown. For the non-Newtonian fluid results there is an increase in the minimum film thickness when compared to the Newtonian results.

The reason for the smaller shift in the transient location of the overall minimum film thickness with diametric clearance though the gait cycle can be attributed to the more distinct single minimum film thickness in the gait cycle for the physiological cycle. Conversely for the joint simulator cycle there are a number of local minima and maxima which only require a small change in the film thickness distribution through

the cycle to occur for a different local minima to become the global minima. This result highlights the importance of careful representation of the rheological model if predictions of wear and/or tribo-corrosion are to be made from the predicted film thickness distribution.

The difference in the central film thickness between the non-Newtonian and Newtonian cases alludes to the differences in the film thicknesses outside the region where the minimum film thickness exists. It is interesting to observe that at the beginning of both gait cycles the central film thickness is significantly larger for the non-Newtonian than for the Newtonian rheological models. The film thickness contours in Figs. 6 and 7 result from the essential differences between the two rheological models considered. It can clearly be observed that, while the minimum film thicknesses may not be significantly different, the larger film thickness away from the region of minimum film thickness region for the non-Newtonian cases are considerably greater than for the Newtonian case. This can be further observed in Fig. 8, which shows a narrower region of low film thicknesses for the non-Newtonian than for the Newtonian cases. Fig. 9 shows how the viscosity of the fluid rises significantly outside the minimum film thickness region.

The importance of the gait cycle is also highlighted in Fig. 10, which shows dramatically how a significantly higher viscosity occurs in the simplified simulator model, where there is an abrupt reversal of motion, compared to the model in which there is always relative motion between the femoral head and the acetabular cup. It should also be noted that, despite the more constant minimum viscosity for the physiological gait cycle data it still varies from 1.06 to 1.65 mPas.

The numerical solutions demonstrate the limitations of a rheological model in which the lubricant viscosity is assumed to be constant and equal to the very high shear rate value for synovial fluid. More complete representations of relative motions

about two axes yield relatively low but finite shear rates during motion reversal. The bearing thus enjoys much longer periods of exposure to low shear rates and hence very much greater viscosities. Much higher film thicknesses are therefore established prior to exposure to the peak loadings. Powerful squeeze-film action significantly maintains higher film thicknesses than could be maintained by an isoviscous lubricant having viscosities little greater than water.

For acetabular cup and femoral heads with identical arithmetic average surface roughness values of 10 nm, the composite root mean square roughness R_a is 14.1 nm. The corresponding maximum and minimum lambda (λ) ratios for both simulator and physiological cycles are shown in Table 2.

$$\lambda = h_{min}/R_a \tag{11}$$

During the past half century or so engineers have found that the lambda ratio (λ) is a simple and very useful parameter for the assessment of lubrication modes and durability of highly stressed lubricated machine components. In general, $\lambda \leq$ I suggests boundary lubrication while λ = 1-2 mixed lubrication and $\lambda \geq 3$ or 4 fluid film lubrication. An examination of the lambda ratios in Table 2 suggests that mixed or boundary lubrication is likely to be encountered in the stance phase for both operating cycles, with a good chance of benefitting from elastohydrodynamic action if the lubricant exhibits non-Newtonian characteristics. In the swing phase the indications are that fluid film lubrication can be expected throughout the swing phases of either cycle whether or not the lubricant exhibits non-Newtonian behavior. In the stance phase mixed lubrication is predicted for the physiological cycle.

These guidelines do not ensure complete separation, which calls for much greater lambda ratios. If lambda ratios are sufficiently large ‘running in’ normally occurs and this empirical guideline has resulted in major advantages in the operation of many lubricated machine elements. The lambda ratios quoted in the present paper simply contribute to the growing bank of information which may eventually prove to be as

valuable to manufactures of metal-on-metal hip joint replacements as lambda ratios have been to the development of safe guidelines for many other, lubricated contacts.

5 Conclusions

The principal aim of this study was to explore the role of rheology, represented by a marked reduction of synovial fluid viscosity with increasing shear rate, in metal-on-metal hip replacements. Two loading and motion cycles, representative of typical joint simulator operating conditions and physiological cycle have been investigated. The findings are;

1. At low shear rates, the non-Newtonian characteristics of synovial fluid increase the calculated film thicknesses substantially. The very high lubricant viscosity at low shear rates is thus responsible for the enhanced values of film thickness.
2. Powerful squeeze-film action maintains higher film thicknesses for the shear dependent viscosity throughout the complete cycles of operation for both operating cycles.
3. The predicted minimum film thickness increase substantially as the clearance decreases, for both Newtonian and non-Newtonian representations of viscosity.
4. The findings demonstrate the importance of clearance and non-Newtonian lubricant rheology in tribological studies of theoretical lubricating film behaviour.
5. The lambda ratios suggest that fluid-film lubrication is likely in the swing phase of both operating cycles, with the possibility of some mixed or boundary lubrication in the stance phases, particularly for the physiological walking cycle.

Acknowledgement

The research leading to these results has received funding from the European

Union's Seventh Framework Programme (FP7/2007-2013) under the LifeLongJoints Project, Grant Agreement No. GA-310477.

Nomenclature

c	Diametrical clearance between cup and head (m)	x,y,z	Cartesian coordinates
dyn	Switch factor to choose between steady state and transient conditions	α	Parameter in Eq. (1)
$e_{x,y,z}$	Eccentricity component (m)	β_0	Angle of cup inclination (rad)
h	Film thickness (m)	β	Power of shear rate in Eq. (1)
K	Displacement influence coefficient (m^3/N)	$\dot{\gamma}$	Shear rate (s^{-1})
p	Pressure (Pa)	δ	Surface elastic deformation (m)
R_C	Cup inside radius (m)	ϕ, θ	Spherical coordinates (rad)
t	Time (s)	η	Viscosity of synovial fluid (Pas)
v_θ, v_φ	Spherical velocity component (m/s)	η_0	Viscosity at zero shear rate (Pas)
v	Relative surface velocity (m/s)	η_∞	Viscosity at infinite shear rate (Pas)
w	Applied load (N)	$\omega_{x,y,z}$	Angular velocity component (rad/s)

REFERENCES

[1] McKee GK, Watson-Farrar J. Replacement of arthritic hips by the McKee-Farrar prosthesis. JBone Jt Surg. 1966;48B:245-59.

[2] Charnley J. Arthroplasty of the hip-a new operation. Lancet. 1961;1:1129-32.

[3] Ingham E, Fisher J. The role of macrophages in osteolysis of total joint replacement. Biomaterials. 2005;26:1271-86.

[4] Langton DJ, Joyce TJ, Jameson SS, Lord J, Van Orsouw M, Holland JP, Nargol AVF, De Smet KA. Adverse reaction to metal debris following hip resurfacing. The influence of component type, orientation and volumetric wear. J Bone Joint Surg Br. 2011;93B:164-71.

[5] Lord JK, Langton DJ, Nargol AVF, Joyce TJ. Volumetric wear assessment of failed metal-on-metal hip resurfacing prostheses. Wear. 2011;272:79-87.

[6] Daniel J, Holland J, Quigley L, Sprague S, Bhandari M. Pseudotumors associated with total hip arthroplasty. J Bone Joint Surg Am. 2012;94A:86-93.

[7] Bal BS, Rahaman MN. Orthopedic applications of silicon nitride ceramics. Acta Biomater. 2012;8:2889-98.

[8] Dowson D, Neville A. In: Revell PA, editor. Tribology and corrosion in hip joint replacements:

materials and engineering, Joint Replacement Technology. Second ed2014. p. 401-42.
[9] Jin ZM, Dowson D. A full numerical analysis of hydrodynamic lubrication in artificial hip joint replacements constructed from hard materials. Proc Inst Mech Eng Part C: J Mech Eng Sci. 1999;213:355-70.
[10] Dowson D, McNie CM, Goldsmith AAJ. Direct experimental evidence of lubrication in a metal-on-metal total hip replacement tested in a joint simulator. Proc Inst Mech Eng Part C: J Mech Eng Sci. 2000;214:75-86.
[11] Myant C, Underwood R, Fan J, Cann PM. Lubrication of metal-on-metal hip joints: The effect of protein content and load on film formation and wear. J Mech Behav Biomed. 2012;6:30-40.
[12] Chan FW, Bobyn JD, Medley JB, Krygier JJ, Tanzer M. The Otto Aufranc Award - Wear and lubrication of metal-on-metal hip implants. Clin Orthop Relat R. 1999;369:10-24.
[13] Gao LM, Wang FC, Yang PR, Jin ZM. Effect of 3D physiological loading and motion on elastohydrodynamic lubrication of metal-on-metal total hip replacements. Med Eng Phys. 2009;31:720-29.
[14] Jin ZM. Theoretical studies of elastohydrodynamic lubrication of artificial hip joints. Proc Inst Mech Eng Part J: J Eng Trib. 2006;220:719-27.
[15] Liu F, Jin ZM, Roberts P, Grigoris P. Effect of bearing geometry and structure support on transient elastohydrodynamic lubrication of metal-on-metal hip implants. J Biomech. 2007;40:1340-49.
[16] Mattei L, Di Puccio F, Piccigallo B, Ciulli E. Lubrication and wear modelling of artificial hip joints: A review. Tribol Int. 2011;44:532-49.
[17] Meyer DM, Tichy JA. 3-D model of a total hip replacement in vivo providing hydrodynamic pressure and film thickness for walking and bicycling. Trans ASME J Biomech Eng. 2003;125:777-84.
[18] Wang FC, Jin ZM. Transient elastohydrodynamic lubrication of hip joint implants. Trans ASME J Tribol. 2008;130:011007.
[19] Williams S, Jalali-Vahid D, Brockett C, Jin ZM, Stone MH, Ingham E, Fisher J. Effect of swing phase load on metal-on-metal hip lubrication, friction and wear. J Biomech. 2006;39:2274-81.
[20] Meng QE, Liu F, Fisher J, Jin ZM. Effect of simplifications of bone and components inclination on the elastohydrodynamic lubrication modeling of metal-on-metal hip resurfacing prosthesis. Proc Inst Mech Eng Part H: J Eng Med. 2013;227:523-34.
[21] Yao JQ, Laurent MP, Johnson TS, Blanchard CR, Crowninshield RD. The influences of lubricant and material on polymer/CoCr sliding friction. Wear. 2003;255:780-84.
[22] Wang WZ, Jin ZM, Dowson D, Hu YZ. A study of the effect of model geometry and lubricant rheology upon the elastohydrodynamic lubrication performance of metal-on-metal hip joints. Proc Inst Mech Eng Part J: J Eng Trib. 2008;222:493-501.
[23] Tichy J, Bou-Said B. The Phan-Thien and tanner model applied to thin film spherical coordinates: Applications for lubrication of hip joint replacement. Trans ASME J Biomech Eng. 2008;130:021012.
[24] Phan-Thien N, Tanner RI. A new constitutive equation derived from network theory. J Non-Newton Fluid. 1977;2:353-65.
[25] Meziane A, Bou-Said B, Tichy J. Modelling human hip joint lubrication subject to walking cycle. Lubr Sci. 2008;20:205-22.
[26] Hesketh J, Meng Q, Dowson D, Neville A. Biotribocorrosion of metal-on-metal hip replacements: How surface degradation can influence metal ion formation. Tribol Int. 2013;65:128-37.
[27] Bergmann G, Deuretzbacher G, Heller M, Graichen F, Rohlmann A, Strauss J, Duda GN. Hip contact forces and gait patterns from routine activities. J Biomech. 2001;34:859-71.

[28] Cooke AV, Dowson D, Wright V. The rheology of synovial fluid and some potential synthetic lubricants for degenerate synovial fluid. Proc Inst Mech Eng Part H: J Eng Med. 1978;7:66-72.
[29] Cross MM. Rheology of non newtonian fuids: A new flow equation for pseudoplastic systems. J Colloid Interf Sci. 1965;20:417-37.
[30] Wang FC, Jin ZM. Prediction of elastic deformation of acetabular cups and femoral heads for lubrication analysis of artificial hip joints. Proc Inst Mech Eng Part J: J Eng Trib. 2004;218:201-09.

Tables and Figures

Table 1 Geometrical and material parameters of a MOM total hip replacement

Table 2Lambda ratios calculated for the joint simulator and physiological operating cycles (diametric clearance = 100 μm)

Fig. 1. An anatomical illustration of MOM hip joint under 3D loading and rotation (flexion/extension, ω_x; internal/external rotation, ω_y; adduction/abduction, ω_z).

Fig. 2. Spherical coordinates for the EHL analysis of the described hip implant.

Fig. 3. a) Load and angular velocity of ProSim hip simulator gait pattern
b) 3-dimensional load of physiological gait pattern, and c) 3-dimensional angular velocity of physiological gait pattern.

Fig. 4. The magnitudes (top) and locations (bottom) of the minimum film thickness against hip joint clearance: (a) hip simulator pattern and (b) physiological pattern.

Fig. 5. Variations of the minimum and central film thickness in a walking cycle as a loop (*cd* = 100 μm): a) and b) for the hip simulator cycle with cup inclination angle of 45 degrees and zero respectively; c) for the physiological walking pattern. The numbers and round dots indicate the maximum or minimum magnitudes and their locations. The arrows show the direction of a walking cycle.

Fig. 6. Film thickness contours at two time steps in a walking cycle of hip simulator pattern (*cd* = 100 μm, horizontal for ϕ direction, vertical for θ direction; unit: degree).

Fig. 7. Film thickness contours at two time steps in a walking cycle of physiological pattern (*cd* = 100 μm, horizontal for ϕ direction, vertical for θ direction).

Fig. 8. Film thickness profile on a cross-section at two time steps in a walking cycle (*cd* = 100 μm): a) hip simulator pattern and b) physiological pattern.

Fig. 9. Non-Newtonian viscosity contours at certain time steps in a walking cycle (*cd* = 100 μm): a) hip simulator pattern at 0.2 s; b) physiological pattern at 0.55 s; and c) physiological pattern at 1.1 s.

Fig. 10. Variations of the minimum viscosity in a walking cycle.

Table 1 Geometrical and material parameters of a MOM total hip replacement

Diametrical clearance, *cd*	50-150 μm
Head radius, R_H	18 mm
Cup wall thickness	9.5 mm
Equivalent support thickness	2 mm
Elastic modulus of metal	210 GPa
Elastic modulus of equivalent support layer	2.27 GPa
Poisson's ratio of metal	0.3
Poisson's ratio of equivalent support layer	0.23
Viscosity of synovial fluid at zero shear rate	40 Pas
Viscosity of synovial fluid at infinite shear rate	0.9 mPas

Table 2 Lambda ratios calculated for the joint simulator and physiological operating cycles (diametric clearance = 100 μm)

	Newtonian Fluid			**Non-Newtonian Fluid**	
Simulator (cup 45 degree)	h_{min}(nm)	Lambda Ratio		h_{min} (nm)	Lambda Ratio
Cyclic maximum	47.7	3.4		59.6	4.2
Cyclic minimum	20.6	1.5		23.4	1.7
Physiological					
Cyclic maximum	37.3	2.6		48.4	3.4
Cyclic minimum	11.9	0.84		16.1	1.1

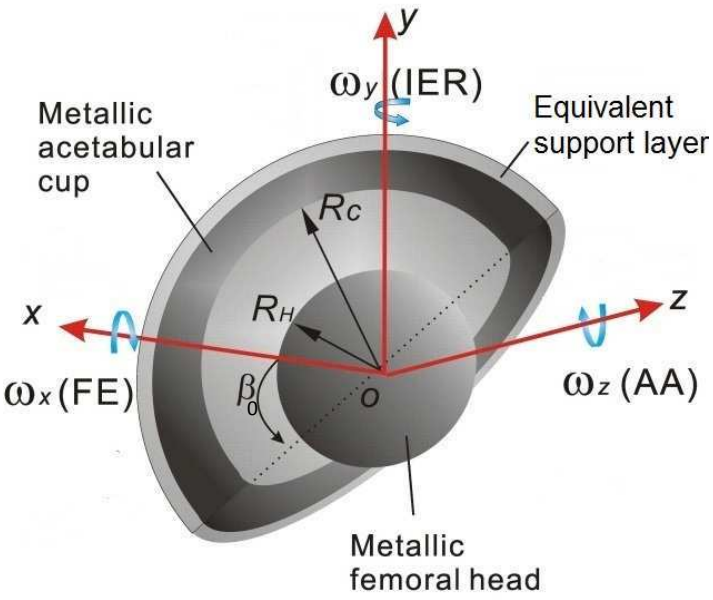

Fig. 1. An anatomical illustration of MOM hip joint under 3D loading and rotation (flexion/extension, ω_x; internal/external rotation, ω_y; adduction/abduction, ω_z).

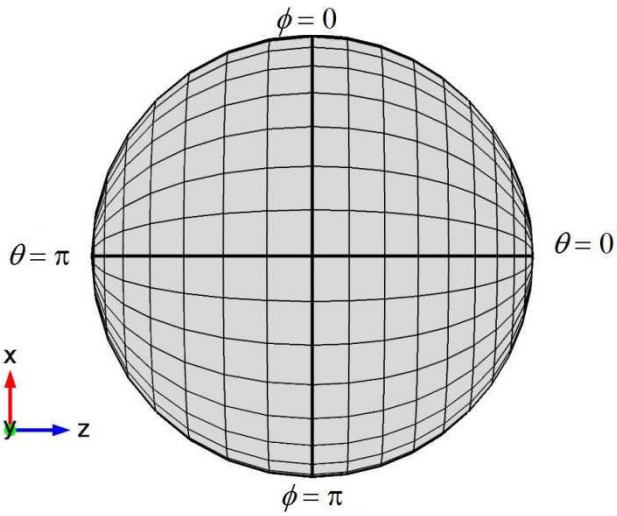

Fig. 2. Spherical coordinates for the EHL analysis of the described hip implant.

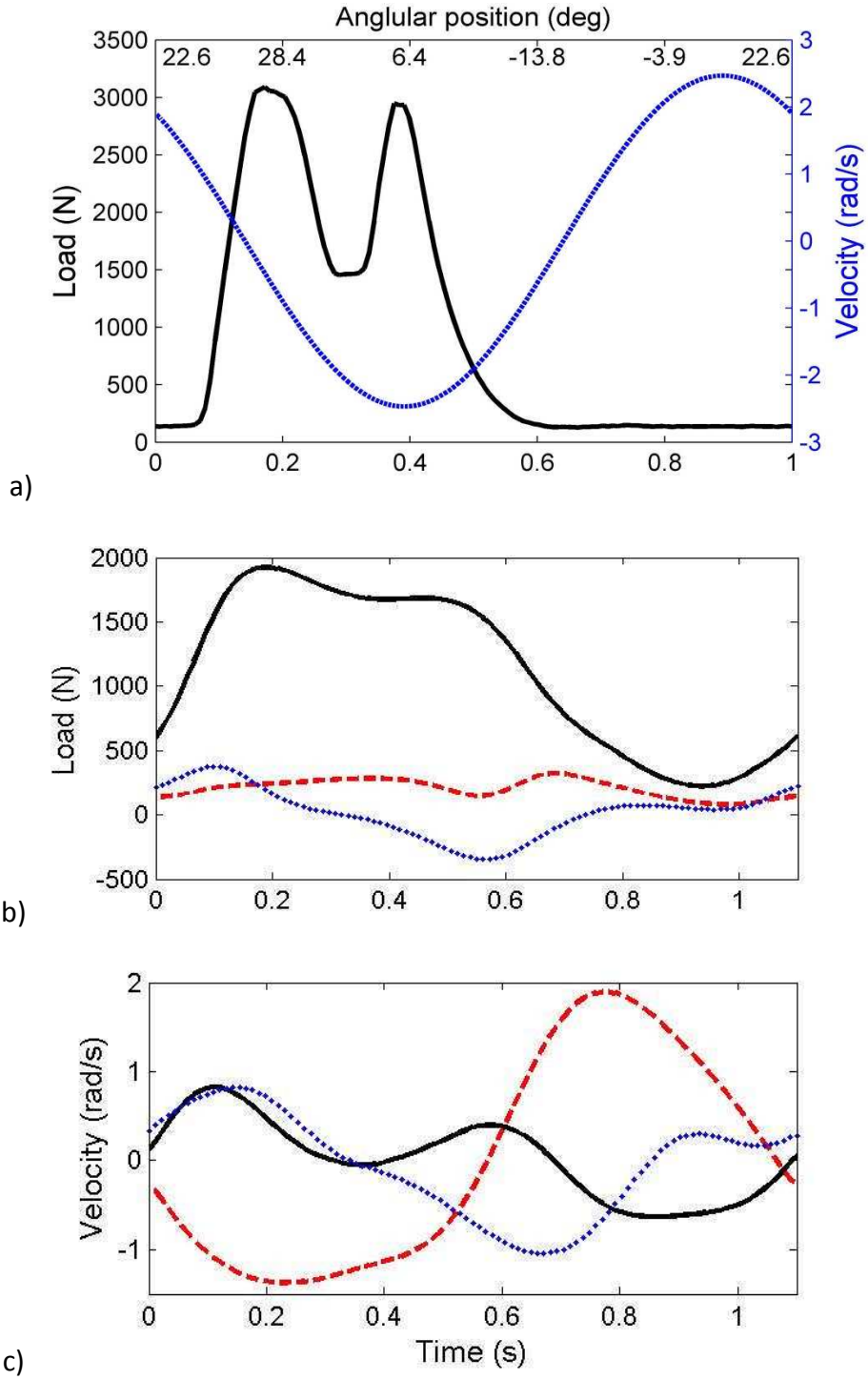

Fig. 3. a) Load and angular velocity of ProSim hip simulator gait pattern
b) 3-dimensional load of physiological gait pattern, and c) 3-dimensional angular velocity of physiological gait pattern.

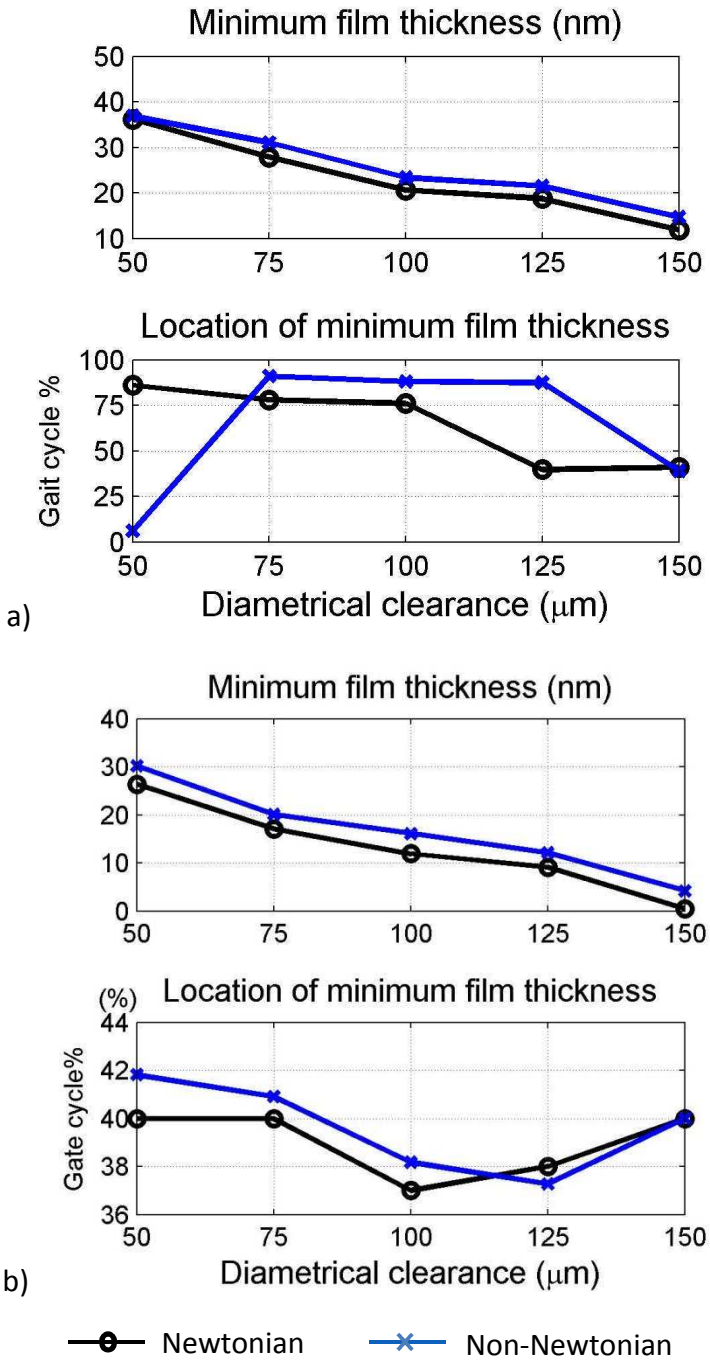

Fig. 4. The magnitudes (top) and locations (bottom) of the minimum film thickness against hip joint clearance: (a) hip simulator pattern and (b) physiological pattern.

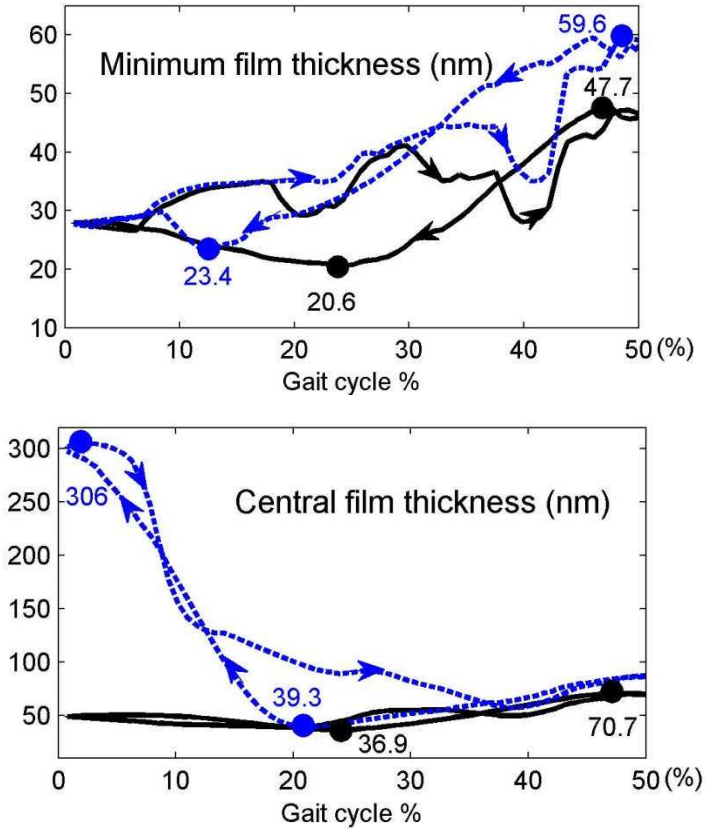

a) hip simulator pattern (cup inclination angle of 45 degrees)

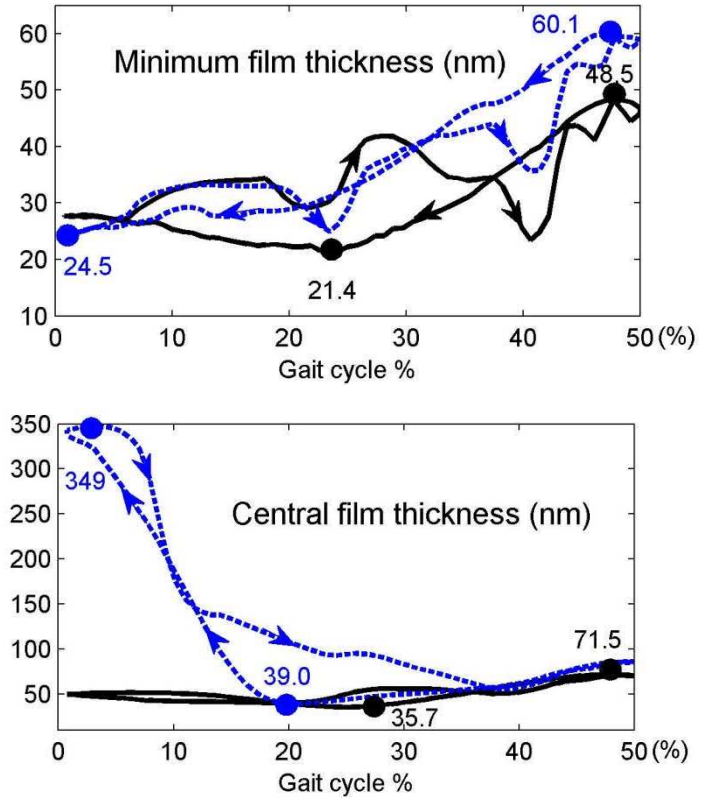

b) hip simulator pattern (cup inclination angle of zero)

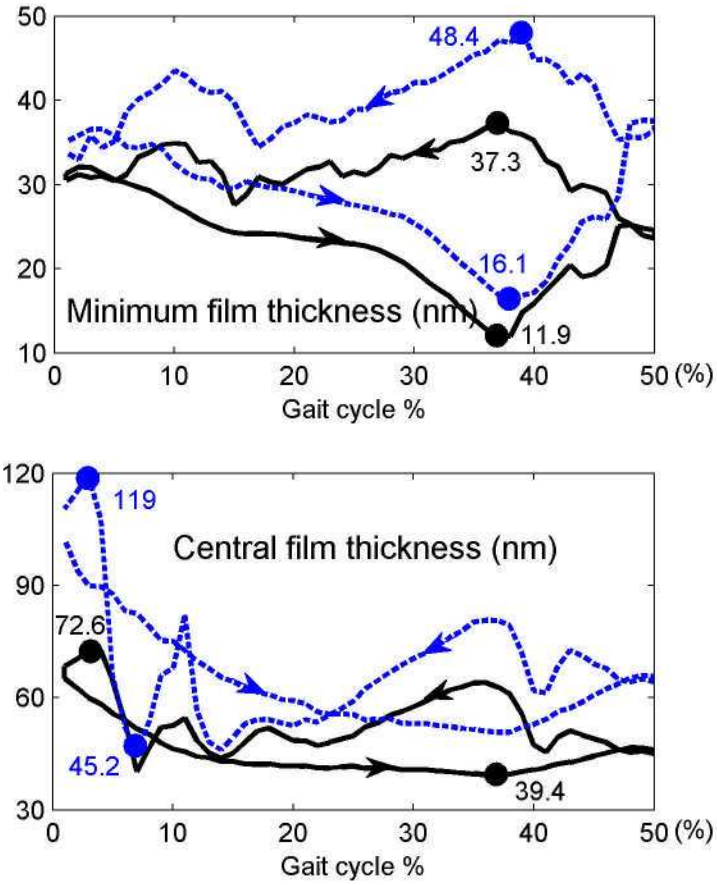

c) Physiological walking pattern

Newtonian Non-Newtonian

Fig. 5. Variations of the minimum and central film thickness in a walking cycle as a loop (*cd* = 100 μm): a) and b) for the hip simulator cycle with cup inclination angle of 45 degrees and zero respectively; c) for the physiological walking pattern with cup inclination angle of 45 degrees. The numbers and round dots indicate the maximum or minimum magnitudes and their locations. The arrows show the direction of a walking cycle.

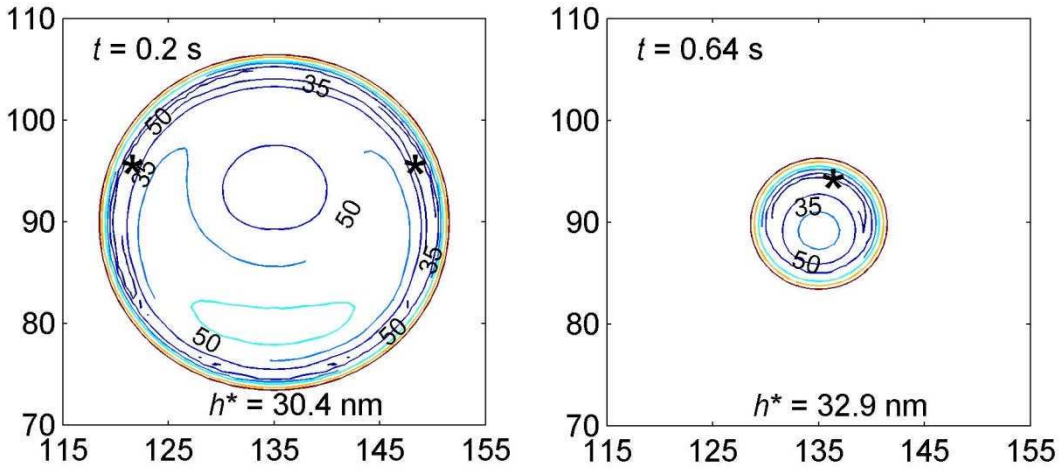

a) Newtonian

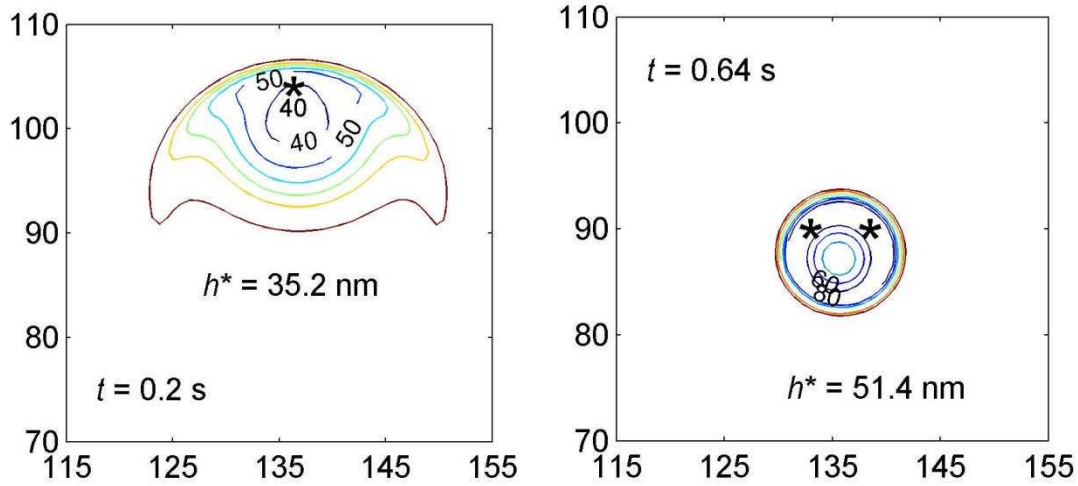

b) non-Newtonian

Fig. 6. Film thickness contours at two time steps in a walking cycle of hip simulator pattern (*cd* = 100 μm, horizontal for ϕ direction, vertical for θ direction; unit: degree).

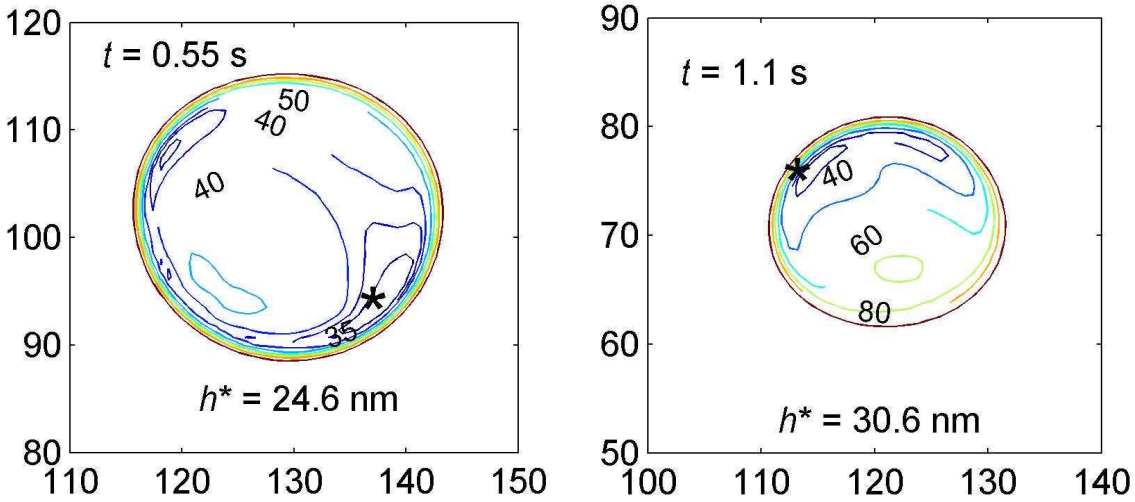

a) Newtonian

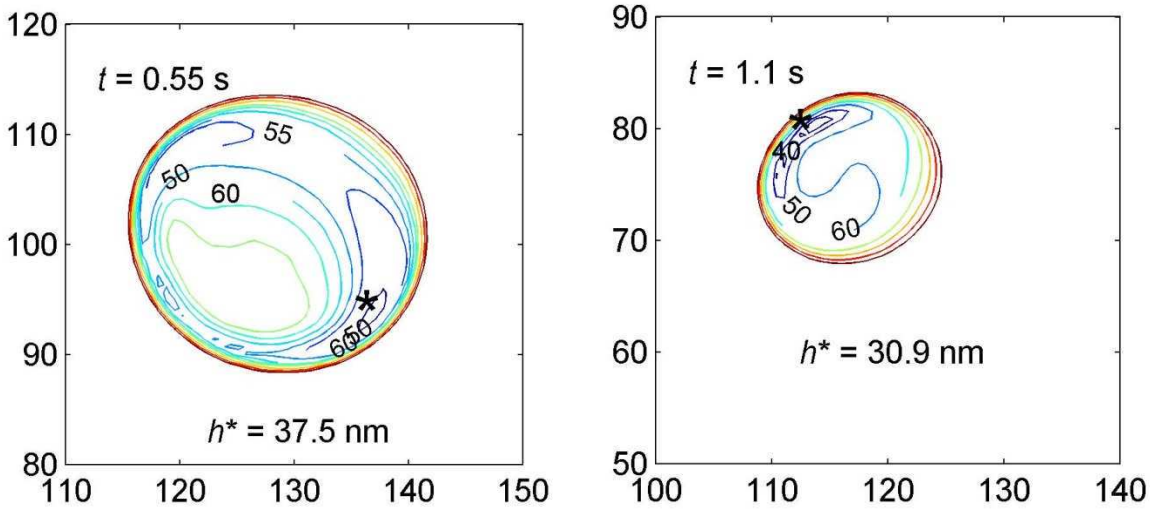

b) non-Newtonian

Fig. 7. Film thickness contours at two time steps in a walking cycle of physiological pattern (*cd* = 100 μm, horizontal for ϕ direction, vertical for θ direction).

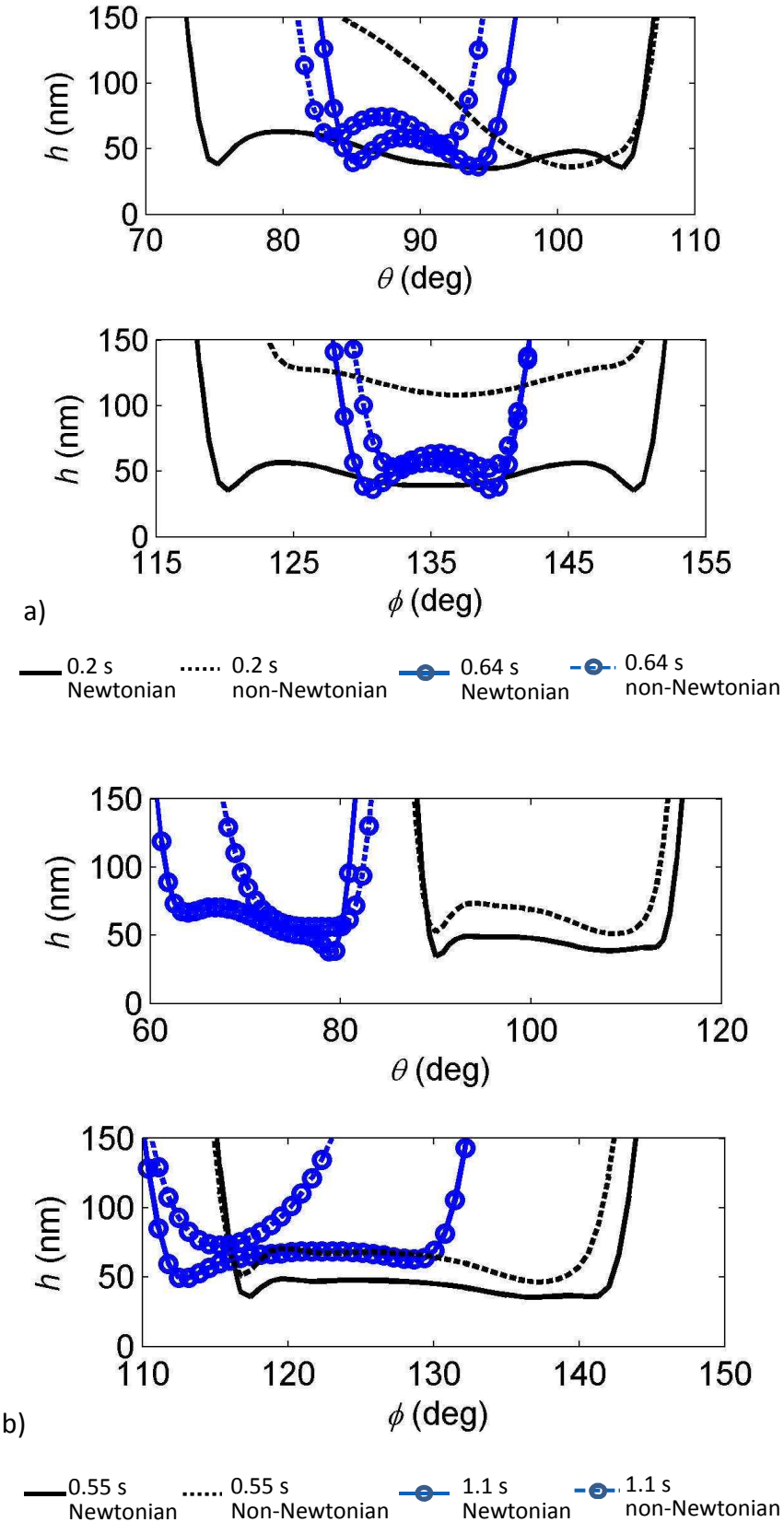

Fig. 8. Film thickness profile on a cross-section at two time steps in a walking cycle (*cd* = 100 μm): a) hip simulator pattern and b) physiological pattern.

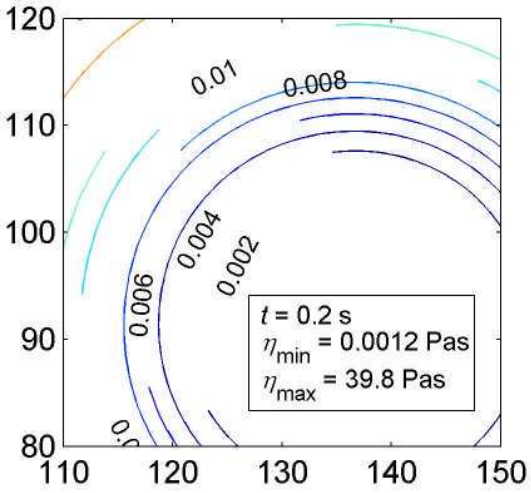

a)

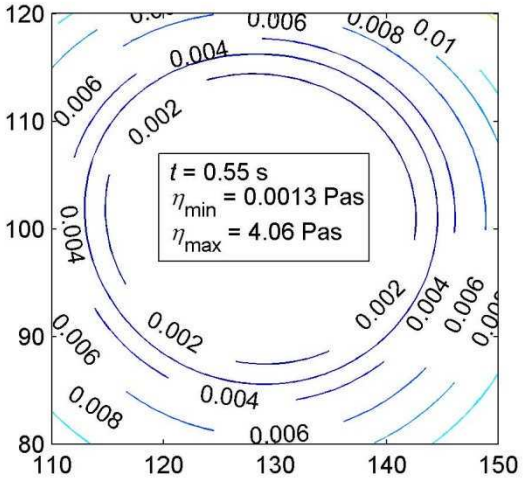

b)

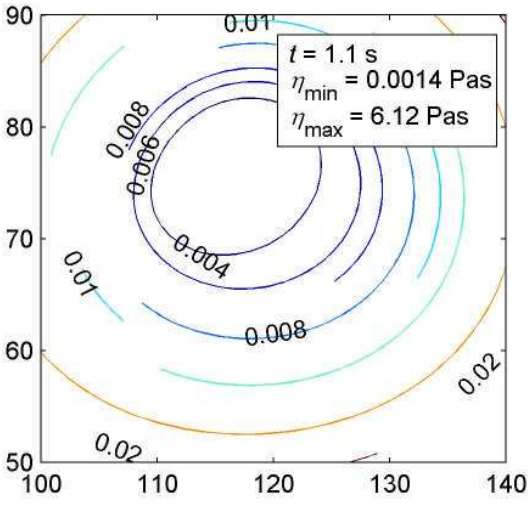

c)

Fig. 9. Non-Newtonian viscosity contours at certain time steps in a walking cycle (*cd* = 100 μm): a) hip simulator pattern at 0.2 s; b) physiological pattern at 0.55 s; and c) physiological pattern at 1.1 s.

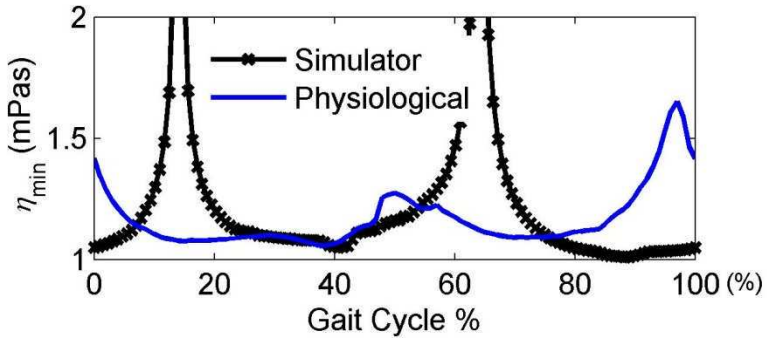

Fig. 10. Variations of the minimum viscosity in a walking cycle (*cd* = 100 μm).